

Self-broadening and self-shift in the $3\nu_2$ band of ammonia from mid-infrared-frequency-comb spectroscopy

Guang Yang,^{1,2} Vinicius Silva de Oliveira,^{2,3} Dominic Laumer,^{2,3} Christoph M. Heyl,^{3,4,5} Andrey Yachmenev,^{1,6} Ingmar Hartl,^{3, a)} and Jochen Küpper^{1,2,6, b)}

¹⁾ Center for Free-Electron Laser Science CFEL, Deutsches Elektronen-Synchrotron DESY, Notkestraße 85, 22607 Hamburg, Germany

²⁾ Department of Physics, Universität Hamburg, Luruper Chaussee 149, 22761 Hamburg, Germany

³⁾ Deutsches Elektronen-Synchrotron DESY, Notkestraße 85, 22607 Hamburg, Germany

⁴⁾ Helmholtz-Institute Jena, Fröbelstieg 3, 07743 Jena, Germany

⁵⁾ GSI Helmholtzzentrum für Schwerionenforschung GmbH, Planckstrasse 1, 64291 Darmstadt, Germany

⁶⁾ Center for Ultrafast Imaging, Universität Hamburg, Luruper Chaussee 149, 22761 Hamburg, Germany

We report the broadband absorption spectrum of the $3\nu_2$ band of $^{14}\text{NH}_3$ near $4\ \mu\text{m}$. The data were recorded using a mid-infrared frequency comb coupled to a homebuilt Fourier-transform spectrometer with a resolution of $0.00501\ \text{cm}^{-1}$. Line positions, line intensities, self-broadening, and self-shift parameters for six rovibrational lines were determined at room temperature ($T = 296\ \text{K}$). Comparison with HITRAN 2016 shows good agreement at improved precision. The high precision and the rapid tunability of our experiment enables advanced fast spectroscopy of molecular gases.

I. INTRODUCTION

Ammonia is one of the spectroscopically most-studied molecules due to its importance in the atmosphere, astrophysics, chemistry, medicine and biology. Ammonia exists in a wide range of astrophysical environments and was the first polyatomic molecule detected in the interstellar medium.¹ It was used as one of the most accurate “molecular thermometers” to measure the temperature of C/2001 Q4(Neat),² 9P/Tempel 1³ and other comets by detecting the *ortho-para* ratio. Ammonia also formed the basis for modern laser technology through the original demonstration of the MASER.⁴ Ammonia spectra have been extensively studied and disentangled, both in theory and experiment.

The spectra of ammonia were extensively measured from the microwave to the ultraviolet.^{5–15} Yurchenko et al.¹⁶ calculated the spectra for ammonia covering a large part of the infrared region using a variational approach. Recently, we calculated hyperfine-resolved rotation-vibration line lists of ammonia,^{17,18} which agree very well with experimental results.¹⁹ The rotation-vibration-spectroscopy data were all critically reviewed and included in the “Measured Active Rotational-Vibrational Energy Levels (MARVEL)” database.²⁰ The high-resolution transmission (HITRAN) molecular absorption database²¹ summarizes the ammonia rotation-vibration spectra, but still has many of the transitions unassigned or absent, especially in the molecular fingerprint region in the mid-infrared (MIR). For instance, there are only two experiments in the $4\ \mu\text{m}$ region, obtained using a Global source¹⁰ and a synchrotron source.¹¹

The development of frequency combs (FC) extended the

traditional gas-phase-absorption spectroscopy to broadband, which allows for the simultaneous detection of multiple transition regions of multiple species in a short acquisition time.²² Coherent MIR-FC light sources allow to precisely measure molecular fingerprints which are useful, e. g., in breath analysis, atmospheric measurements, and astrochemistry.²² Taking breath analysis for an example, ammonia sensing in exhaled human breath could be an indicator of liver and renal diseases.²³ Non-linear frequency conversion approaches utilizing optical parametric oscillators (OPO),^{24–26} optical parametric amplification (OPA),²⁷ supercontinuum generation,^{28,29} or difference frequency generation (DFG)^{30,31} provide an alternative approach to generate optical frequencies in MIR regions which are not covered by laser gain media. MIR FC sources based on DFG are widely used due to their simplicity, single-pass configuration, broad tunability, and full cancellation of the carrier-envelope offset. The combination of a MIR FC with a Fourier transform spectrometer (FTS) offers capabilities to record spectra over a broadband range and with high resolution, high sensitivity, and especially a high signal-to-noise ratio (SNR) due to the high spectral brightness and temporal coherence of FCs.^{24–26}

Here, we report the absorption spectrum of the $3\nu_2$ band of $^{14}\text{NH}_3$ near $4\ \mu\text{m}$ by a homebuilt FTS coupled to a DFG-based MIR FC covering the range $3\text{--}6\ \mu\text{m}$. We extract the transition wavenumbers and intensities for 6 typical *R* branch rovibrational lines through a multipeak Voigt fit at room temperature (296 K). We also retrieve self-broadening- and self-shift-parameters of the pressure interactions in the gas at nine different pressures ranging from 10.00 mbar to 700.00 mbar.

II. EXPERIMENT

A schematic diagram of the experimental setup is shown in Fig. 1. It consists of three parts: the DFG-based MIR

^{a)}Email: ingmar.hartl@desy.de

^{b)}Email: jochen.kuepper@cfel.de; website: <https://www.controlled-molecule-imaging.org>

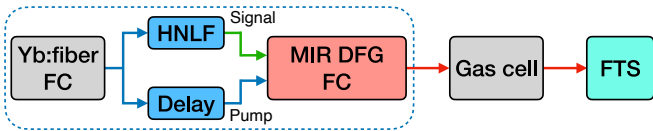


FIG. 1. Generic schematic of experimental setup. FC: frequency comb, HNLFC: highly-nonlinear suspended core-fiber, MIR DFG FC: DFG-based mid-infrared FC, FTS: Fourier transform spectrometer.

FC source, the gas cell, and the FTS. The MIR FC source consists of a Yb:fiber FC and a DFG setup.^{30,32} The Yb:fiber FC is mode-locked by a saturable absorber with the repetition rate of 150 MHz and phase-locked to a cw laser (Coherent Mephisto) with kHz-level linewidth at ~ 1064 nm and frequency stability to 1 MHz/minute. Using chirped-pulse amplification, 1.5 W average power is delivered in pulses of 130 fs duration with a center wavelength of 1050 nm and a bandwidth of 25 nm. The Yb:fiber FC is split into pump and signal driver of the DFG process, with the signal generated as the longest Raman soliton from the supercontinuum process in a highly-nonlinear suspended core-fiber.³³ By controlling the input power, we could adjust the wavelength of the longest Raman soliton from 1.2 μm to 1.6 μm . The signal and pump pulse are temporally overlapped in a fan-out periodically poled Lithium Niobate (PPLN) crystal (HCPhotonics) for DFG by locking a mechanical delay-line in the pump arm.³² This yielded MIR radiation ranging from 3 μm to 6 μm . The MIR FC was tuned to near 4 μm (2390 cm^{-1} to 2510 cm^{-1}), and the light passed through the gas cell together with a frequency stabilized (1 MHz/minute) HeNe laser (SIOS SL4), which was used to calibrate the absolute frequency of the spectroscopic signals.

Ammonia ($^{14}\text{NH}_3$, Linde HiQ 6.0) was contained in a 35.4646(12) mm long gas cell with wedged CaF_2 windows (30 arcmin) at 296 K. The optical path length was determined using low-coherence interferometry³⁴ utilizing the residual 1050 nm laser light from the DFG process as the input signal. The optical path difference (OPD) of the four reflected beams from the two gas cell windows are detected by interfering the reflections with a reference laser. Before the measurements, the reservoir was pumped (HiCube 80 Eco) to $< 3.1 \times 10^{-4}$ mbar, filled to 699.75 mbar of ammonia, and then pumped to 543.85 mbar, 500.01 mbar, 400.50 mbar, 300.70 mbar, 199.90 mbar, 98.90 mbar, 50.00 mbar, and 10.00 mbar, respectively. All pressures were measured using calibrated ceramic capacitance gauges (Pfeiffer Vacuum CMR 361 and CMR 364) with a relative accuracy of 0.2%.

The two laser were both directed to our homebuilt FTS, which is based on a Michelson interferometer with two liquid-nitrogen-cooled indium antimonide (InSb) detector (InfraRed Associates IRA 20-00060). The interferograms of both MIR FC and HeNe laser were acquired at 5 MSa/s sampling rate with 20 bit resolution by a

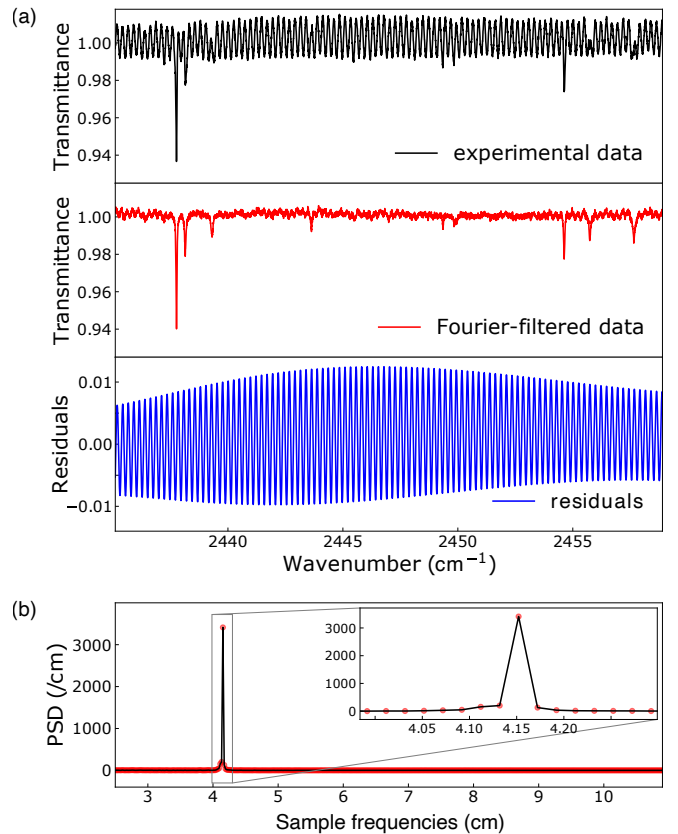


FIG. 2. (a) The absorption spectra at 98.90 mbar and at room temperature (296 K). The top panel shows the experimentally recorded original spectrum. The middle plot shows the spectra after FFT-filtering. The bottom plot shows the residual differences of the two upper spectra. (b) Partial Power Spectral Density (PSD) of the absorption spectrum in (a).

computer-controlled data acquisition board (National Instruments PCI-5922). The interferogram of the HeNe laser was used to measure the OPD and provides steps to resample the MIR FC interferogram by determining the positions of the zero-crossings. By matching the delay range of the FTS to the repetition rate of the MIR FC, we overcame the resolution limitation of conventional FTS given by the maximum delay range and removed the instrumental line shape oscillations, which allowed a reduction of the instrument size and acquisition time.³⁵ The grid spacing was equal to the comb spacing of 150 MHz, yielding a resolution of the FTS of 0.00501 cm^{-1} . After performing a fast Fourier transform (FFT) to MIR FC interferograms, we obtained MIR absorption spectra of ammonia at the different specified pressures. To extract the transmittance, we first measured the reference spectra before filling ammonia when the reservoir was under vacuum.

The top panel of Fig. 2 a shows the raw spectrum in the range 2434 to 2459 cm^{-1} at 98.90 mbar and at 296 K. The recorded spectra had oscillatory background signals (black curve in Fig. 2 a) that not only decreased the SNR

of the spectra, but also changed the center and linewidth of the absorption line profiles. We assigned this regular signal to etalon effects of the optical components in the experimental setup. In order to remove this etalon signal, we used a numerical approach based on FFT analysis. Firstly, we calculated the power spectral density (PSD) for different FFT sample frequencies of the spectra, shown in Fig. 2 b. The unit of sample frequencies was in cm, which exactly corresponded to the OPD of the FTS. Then we set the FFT values for the four sample frequencies between 4.10 cm and 4.18 cm to be zero, and performed an inverse FFT, resulting in the filtered spectrum shown in Fig. 2 a, middle panel. Analyzing the sample frequencies of the filtered signal, Fig. 2 a, bottom panel, we suppose that the etalon signal most likely comes from a Germanium (Ge) filter in the experimental setup; the length and refractive index of the Ge filter at 4 μm are around 5 mm and 4, resulting in a 4 cm OPD that matches the free spectral range of these oscillations. The FFT filtering might have introduced some small errors as the filtered frequencies also included real spectral information. Nevertheless, these errors should be smaller than profile fitting error and the approach clearly improved the precision and SNR. In the future, the Ge filter shall be replaced by wedged optics.

III. RESULTS AND DISCUSSION

Direct multipeak Voigt fit for the transmittance data was performed to retrieve spectral information. Voigt profile was still valid because the transmittance was more than 90% for all transitions due to the low sensitivity with the short gas cell and the pressures of gas sample were relatively high.³⁷ The four basic spectroscopic line parameters – the pressure-broadening $\gamma_{p,t}$, the Doppler-broadening α_D , line transition frequency ν_{ij} , and the spectral line intensity I_{ij} – were determined from individual spectra to extract details on the molecular motions and collisions through a non-linear least-squares fit. Since α_D depends on ν_{ij} and temperature, which was 296 K here, we could reduce the Voigt fit to the three other parameters, as shown in Equation 1.

$$T(\nu) = e^{I_{ij}(T)Nl_{path}V(\nu-\nu_{ij},\gamma_{p,t})} + a_0 \quad (1)$$

Here, N is the number density of ammonia, equals to p/k_bT assuming the ideal gas law, and l_{path} is the optical path length (35.4646 mm in our experiment). In addition, small instrumental baseline a_0 was added in the fit. We assumed a_0 to be a constant value around 0 since the low sensitivity, more general baseline fitting process could be found from Ref. 37.

For the fit we chose six typical peaks with high absorption, corresponding to the $aR(2, K)$ and $aR(3, K)$ multiplets in the $3\nu_2$ band. In order to show the performance of the fit, we show the $aR(2, K)$ multiplet in Fig. 3, which fit very well. The small dip at the low-wavenumber

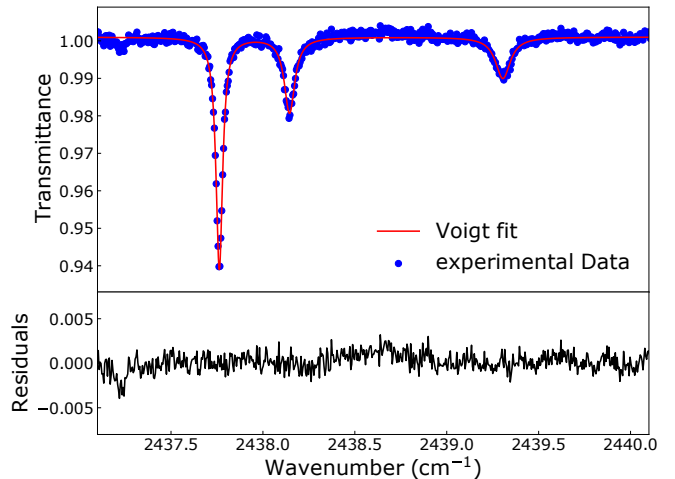


FIG. 3. Results of the non-linear least-squares fit of the $aR(2, K)$ multiplet assuming Voigt line profiles; $K = 0 \dots 2$ correspond to the peaks from left to right. Blue dots depict the experimental spectrum, the red line depicts our multipeak Voigt fit. The lower panel shows the residual difference between experiment and simulation, the noise level is around 0.001.

end of the residual difference corresponds to a $sP(6, 1)$ transition in $\nu_2 + \nu_4$ band. From the fit, we obtained the line-transition frequencies ν_{ij} , line intensities I_{ij} , and the pressure-broadening component $\gamma_{p,t}$, specifically the self-broadening component γ_{self} since the gas cell only contained pure $^{14}\text{NH}_3$.

We recorded and averaged 25 spectra at each of the nine different pressures ranging from 10.00 mbar to 700.00 mbar. It took around 1 minute for recording the spectra and pressures stayed the same during the 25 measurements. Fig. 4 shows the performance of the global multipeak Voigt fit and the extraction of self-broadening and self-shift coefficients for the $aR(2, 0)$ transition. For each pressure, ν_{ij} , I_{ij} and γ_{self} were determined as described above. The mean value of I_{ij} and γ_{self} was extracted. From a linear regression of the line transition wavenumbers ν_{ij} as a function of pressure, see Fig. 4, the vacuum transition wavenumber ν_{ij}^0 was determined as the y intercept and its self-shift parameter γ_{self} as the slope k .

Line wavenumbers ν_{ij}^0 , line intensities I_{ij} , self-broadening γ_{self} , and self-shift δ_{self} components of the $aR(2, K)$ and $aR(3, K)$ multiplet in the $3\nu_2$ band of $^{14}\text{NH}_3$ are presented in Table I. Specified uncertainties for line wavenumbers and self-shifts are their standard deviations from the fit, the uncertainties for line intensities and self-broadenings were the combination of statistical errors from the averaging of multiple scans and the standard deviations from the fit. Other systematic errors such as misalignments of the HeNe laser and MIR FC, the line mixing, the FFT filter etc. were neglected because they were relatively small in relation to the errors from the fit. Line-transition wavenumbers and intensities show good agreement with the HITRAN database values.²¹ Our

TABLE I. Line transitions, line intensities, self-broadening, and self-shift coefficients for the $3\nu_2$ band of $^{14}\text{NH}_3$ at 296 K.

Transition (R branch)	ν_{ij}^0 , exp. (cm^{-1})	ν_{ij} , ref. ^a (cm^{-1})	I_{ij} , exp. ($\text{cm}/\text{molec.}$)	I_{ij} , ref. ^a ($\text{cm}/\text{molec.}$)	$\gamma_{\text{self exp.}}$ ($\text{cm}^{-1}/\text{atm}$)	$\gamma_{\text{self ref.}}^{\text{a}}$ ($\text{cm}^{-1}/\text{atm}$)	δ_{self} ($\text{cm}^{-1}/\text{atm}$)
$aR(2, 0)$	2437.76258(18)	2437.7655	$5.12(19) \times 10^{-22}$	4.590×10^{-22}	0.225(13)	0.302	0.0016(5)
$aR(2, 1)$	2438.14454(106)	2438.1475	$2.35(21) \times 10^{-22}$	2.078×10^{-22}	0.320(33)	0.396	-0.0112(28)
$aR(2, 2)$	2439.31026(421)	2439.3148	$1.70(20) \times 10^{-22}$	1.372×10^{-22}	0.445(63)	0.496	-0.0139(110)
$aR(3, 1)$	2454.62688(68)	2454.6298	$2.26(16) \times 10^{-22}$	2.323×10^{-22}	0.263(31)	0.36	-0.0073(18)
$aR(3, 2)$	2455.73934(231)	2455.7392	$1.93(15) \times 10^{-22}$	1.963×10^{-22}	0.397(43)	0.448	0.0006(62)
$aR(3, 3)$	2457.66341(317)	2457.6615	$2.27(21) \times 10^{-22}$	2.508×10^{-22}	0.464(62)	0.541	-0.0351(83)

^a Data from the HITRAN 2016 database [10, 21, 36], the uncertainty range for ν_0 , I_{ij} and γ_{self} are 0.0001 cm^{-1} to 0.001 cm^{-1} , 10% to 20%, and 2% to 5%, respectively.

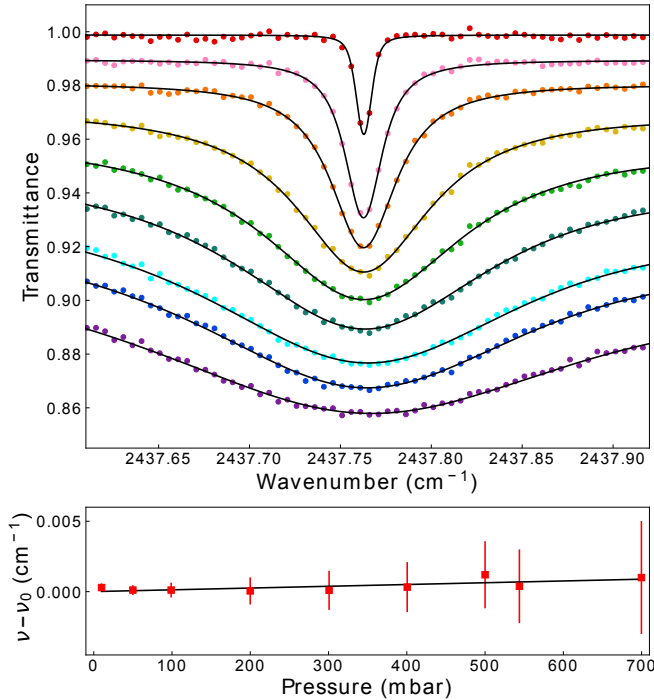


FIG. 4. Extraction of the self-broadening and self-shift parameters from the lineshape of the $aR(2, 0)$ transition at various pressures, i. e., from top to bottom 10.00 mbar, 50.00 mbar, 98.90 mbar, 199.90 mbar, 300.70 mbar, 400.50 mbar, 500.01 mbar, 543.85 mbar, and 699.75 mbar, respectively. The black curves show the fitted Voigt profiles. For clarity, all lines are successively offset by -0.01 from top to bottom. The bottom panel shows the relative line transition wavenumbers (red squares) with respect to the vacuum line transition. Error bars depict the standard deviation from the multipeak Voigt fit. The black line is a linear fit of these transition frequencies from which the vacuum transition wavenumber and the self-shift are derived.

retrieved self-broadening parameters were around 20% smaller than in the HITRAN database, which were derived from measurements at $10 \mu\text{m}$.³⁶ Our results provide new laboratory data allowing to improve pressure-self-broadening models.

IV. CONCLUSIONS

We recorded the broadband absorption spectra of the $3\nu_2$ band of ammonia ($^{14}\text{NH}_3$) near $4 \mu\text{m}$ using a MIR-FC-based FTS system. Spectra were background corrected by FFT-filtering raw spectra for experimental etalon. A global multipeak Voigt fit allowed us to determine transition wavenumbers and intensities, pressure self-broadening and self-shift parameters at room temperature ($T = 296 \text{ K}$) for 6 prototypical R branch rovibrational transitions.

The recorded line wavenumbers and line intensities are in good agreement with the HITRAN database. As no literature values were available for the self-broadening and self-shift parameters, our new experimental data on these parameters provide useful information about the molecular motions and collisions, which could help to improve their theoretical modeling.

Our experimental system is capable of trace-gas detection of different molecular species in the spectral range of $3 \dots 6 \mu\text{m}$ with a current resolution of 0.00501 cm^{-1} . We plan to implement a liquid-nitrogen-cooled multi-pass-cell cryostat to increase the sensitivity.

V. ACKNOWLEDGMENTS

We acknowledge support by Deutsches Elektronen-Synchrotron DESY, a member of the Helmholtz Association (HGF), and through the Maxwell computational resources operated at Deutsches Elektronen-Synchrotron DESY, Hamburg, Germany. This work was further supported by the Deutsche Forschungsgemeinschaft (DFG) through the priority program “Quantum Dynamics in Tailored Intense Fields” (QUTIF, SPP1840, YA 610/1) and the cluster of excellence “Advanced Imaging of Matter” (AIM, EXC 2056, ID 390715994). G.Y. gratefully acknowledges financial support from the China Scholarship Council (CSC).

- ¹A. C. Cheung, D. M. Rank, C. H. Townes, D. D. Thornton, and W. J. Welch, "Detection of NH_3 molecules in the interstellar medium by their microwave emission," *Phys. Rev. Lett.* **21**, 1701–1705 (1968).
- ²H. Kawakita, N. D. Russo, R. Furusho, T. Fuse, J. Watanabe, D. C. Boice, K. Sadakane, N. Arimoto, M. Ohkubo, and T. Ohnishi, "Ortho-to-para ratios of water and ammonia in comet C/2001 Q4 (NEAT): Comparison of nuclear spin temperatures of water, ammonia, and methane," *Astrophys. J.* **643**, 1337–1344 (2006).
- ³H. Kawakita, E. Jehin, J. Manfroid, and D. Hutsemékers, "Nuclear spin temperature of ammonia in comet 9P/Tempel 1 before and after the deep impact event," *Icarus* **191**, 513–516 (2007).
- ⁴J. P. Gordon, H. J. Zeiger, and C. H. Townes, "The Maser—new type of microwave amplifier, frequency standard, and spectrometer," *Phys. Rev.* **99**, 1264–1274 (1955).
- ⁵J. P. Gordon, H. J. Zeiger, and C. H. Townes, "Molecular microwave oscillator and new hyperfine structure in the microwave spectrum of NH_3 ," *Phys. Rev.* **95**, 282–284 (1954).
- ⁶S. Urban, V. Špirko, D. Papoušek, J. Kauppinen, S. P. Belov, L. I. Gershtein, and A. F. Krupnov, "A simultaneous analysis of the microwave, submillimeterwave, far infrared, and infrared-microwave two-photon transitions between the ground and ν_2 inversion-rotation levels of $^{14}\text{NH}_3$," *J. Mol. Spectrosc.* **88**, 274–292 (1981).
- ⁷B. J. Drouin, S. Yu, J. C. Pearson, and H. Gupta, "Terahertz spectroscopy for space applications: 2.5–2.7 THz spectra of HD, H_2O and NH_3 ," *J. Mol. Spectrosc.* **1006**, 2–12 (2011).
- ⁸J. J. Hillman, D. E. Jennings, and J. L. Faris, "Diode laser- CO_2 laser heterodyne spectrometer: measurement of $2sQ(1,1)$ in $2\nu_2-\nu_2$ of NH_3 ," *Appl. Opt.* **18**, 1808–1811 (1979).
- ⁹C. Cottaz, G. Tarrago, I. Kleiner, and L. R. Brown, "Assignments and intensities of $^{14}\text{NH}_3$ hot bands in the 5- to 8- μm ($3\nu_2-\nu_2$, $\nu_2+\nu_4-\nu_2$) and 4- μm ($4\nu_2-\nu_2$, $\nu_1-\nu_2$, $\nu_3-\nu_2$ and $2\nu_4-\nu_2$) regions," *J. Mol. Spectrosc.* **209**, 30–49 (2001).
- ¹⁰I. Kleiner, G. Tarrago, and L. R. Brown, "Positions and intensities in the $3\nu_2/\nu_2 + \nu_4$ vibrational system of $^{14}\text{NH}_3$ near 4 μm ," *J. Mol. Struct.* **173**, 120–145 (1995).
- ¹¹J. Pearson, S. Yu, J. Pearson, K. Sung, B. Drouin, and O. Pirali, "Extended measurements and an experimental accuracy effective Hamiltonian model for the $3\nu_2$ and $\nu_4 + \nu_2$ states of ammonia," *J. Mol. Spectrosc.* **353**, 60–66 (2018).
- ¹²L. Li, R. M. Lees, and L.-H. Xu, "External cavity tunable diode laser spectra of the $\nu_1 + 2\nu_4$ stretch-bend combination bands of $^{14}\text{NH}_3$ and $^{15}\text{NH}_3$," *J. Mol. Spectrosc.* **243**, 219–226 (2007).
- ¹³S. R. Langford, A. J. Orr-Ewing, R. A. Morgan, C. M. Western, M. N. R. Ashfold, A. Rijkenberg, C. R. Scheper, W. J. Buma, and C. A. de Lange, "The spectroscopy of high Rydberg states of ammonia," *J. Chem. Phys.* **108**, 6667–6680 (1998).
- ¹⁴A. E. Douglas, "Electronically excited states of ammonia," *Discuss. Faraday Soc.* **35**, 158–174 (1963).
- ¹⁵J. van Veldhoven, J. Küpper, H. L. Bethlem, B. Sartakov, A. J. A. van Rooij, and G. Meijer, "Decelerated molecular beams for high-resolution spectroscopy: The hyperfine structure of $^{15}\text{ND}_3$," *Eur. Phys. J. D* **31**, 337–349 (2004).
- ¹⁶S. N. Yurchenko, R. J. Barber, A. Yachmenev, W. Thiel, P. Jensen, and J. Tennyson, "A variationally computed $T = 300$ K line list for NH_3 ," *J. Phys. Chem. A* **113**, 11845–11855 (2009).
- ¹⁷A. Yachmenev and J. Küpper, "Communication: General variational approach to nuclear-quadrupole coupling in rovibrational spectra of polyatomic molecules," *J. Chem. Phys.* **147**, 141101 (2017), arXiv:1709.08558 [physics].
- ¹⁸P. Coles, A. Owens, J. Küpper, and A. Yachmenev, "Hyperfine-resolved rotation-vibration line list of ammonia (NH_3)," *Astrophys. J.* **870**, 24 (2018), arXiv:1809.06915 [physics].
- ¹⁹S. Twagirayezu, G. E. Hall, and T. J. Sears, "Quadrupole splittings in the near-infrared spectrum of $^{14}\text{NH}_3$," *J. Chem. Phys.* **145**, 144302 (2016).
- ²⁰A. R. Al Derzi, T. Furtenbacher, J. Tennyson, S. N. Yurchenko, and A. G. Császár, "Marvel analysis of the measured high-resolution spectra of $^{14}\text{NH}_3$," *J. Quant. Spectrosc. Radiat. Transf.* **161**, 117–130 (2015).
- ²¹I. Gordon, L. Rothman, C. Hill, R. Kochanov, Y. Tan, P. Bernath, M. Birk, V. Boudon, A. Campargue, K. Chance, B. Drouin, J.-M. Flaud, R. Gamache, J. Hodges, D. Jacquemart, V. Perevalov, A. Perrin, K. Shine, M.-A. Smith, J. Tennyson, G. Toon, H. Tran, V. Tyuterev, A. Barbe, A. Császár, V. Devi, T. Furtenbacher, J. Harrison, J.-M. Hartmann, A. Jolly, T. Johnson, T. Karman, I. Kleiner, A. Kyuberis, J. Loos, O. Lyulin, S. Massie, S. Mikhailenko, N. Moazzen-Ahmadi, H. Müller, O. Naumenko, A. Nikitin, O. Polyansky, M. Rey, M. Rotger, S. Sharpe, K. Sung, E. Starikova, S. Tashkun, J. V. Auwera, G. Wagner, J. Wilzewski, P. Wcisło, S. Yu, and E. Zak, "The HITRAN2016 molecular spectroscopic database," *J. Quant. Spectrosc. Radiat. Transf.* **203**, 3–69 (2017).
- ²²K. C. Cossel, E. M. Waxman, I. A. Finneran, G. A. Blake, J. Ye, and N. R. Newbury, "Gas-phase broadband spectroscopy using active sources: progress, status, and applications," *J. Opt. Soc. Am. B* **34**, 104–129 (2017).
- ²³M. W. Signets, "High-resolution infrared laser spectroscopy and gas sensing applications," in *Handbook of High-resolution Spectroscopy* (John Wiley & Sons, 2011).
- ²⁴K. A. Tillman, R. R. J. Maier, D. T. Reid, and E. D. McNaghten, "Mid-infrared absorption spectroscopy across a 14.4 THz spectral range using a broadband femtosecond optical parametric oscillator," *Appl. Phys. Lett.* **85**, 3366–3368 (2004).
- ²⁵Ł. Kornaszewski, N. Gayraud, J. M. Stone, W. N. MacPherson, A. K. George, J. C. Knight, D. P. Hand, and D. T. Reid, "Mid-infrared methane detection in a photonic bandgap fiber using a broadband optical parametric oscillator," *Opt. Exp.* **15**, 11219–11224 (2007).
- ²⁶F. Adler, P. Masłowski, A. Foltynowicz, K. C. Cossel, T. C. Briles, I. Hartl, and J. Ye, "Mid-infrared fourier transform spectroscopy with a broadband frequency comb," *Opt. Exp.* **18**, 21861–21872 (2010).
- ²⁷Z. Heiner, V. Petrov, G. Steinmeyer, M. J. J. Vrakking, and M. Mero, "100-kHz, dual-beam OPA delivering high-quality, 5-cycle angular-dispersion-compensated mid-infrared idler pulses at 3.1 μm ," *Opt. Express* **26**, 25793–25804 (2018).
- ²⁸T. Cheng, K. Nagasaka, T. H. Tuan, X. Xue, M. Matsumoto, H. Tezuka, T. Suzuki, and Y. Ohishi, "Mid-infrared supercontinuum generation spanning 2.0 to 15.1 μm in a chalcogenide step-index fiber," *Opt. Lett.* **41**, 2117–2120 (2016).
- ²⁹Z. Zhao, X. Wang, S. Dai, Z. Pan, S. Liu, L. Sun, P. Zhang, Z. Liu, Q. Nie, X. Shen, and R. Wang, "1.5–14 μm midinfrared supercontinuum generation in a low-loss Te-based chalcogenide step-index fiber," *Opt. Lett.* **41**, 5222–5225 (2016).
- ³⁰A. Ruehl, A. Gambetta, I. Hartl, M. E. Fermann, K. S. E. Eikema, and M. Marangoni, "Widely-tunable mid-infrared frequency comb source based on difference frequency generation," *Opt. Lett.* **37**, 2232–2234 (2012).
- ³¹G. Soboń, T. Martynkien, P. Mergo, L. Rutkowski, and A. Foltynowicz, "High-power frequency comb source tunable from 2.7 to 4.2 μm based on difference frequency generation pumped by an Yb-doped fiber laser," *Opt. Lett.* **42**, 1748–1751 (2017).
- ³²V. S. de Oliveira, A. Ruehl, P. Masłowski, and I. Hartl, "Intensity noise optimization of a mid-infrared frequency comb difference-frequency generation source," *Opt. Lett.* **45**, 1914–1917 (2020).
- ³³L. Dong, B. K. Thomas, and L. Fu, "Highly nonlinear silica suspended core fibers," *Opt. Exp.* **16**, 16423–16430 (2008).
- ³⁴I. Hartl, X. D. Li, C. Chudoba, R. K. Ghanta, T. H. Ko, J. G. Fujimoto, J. K. Ranka, and R. S. Windeler, "Ultrahigh-resolution optical coherence tomography using continuum generation in an air-silica microstructure optical fiber," *Opt. Lett.* **26**, 608–610 (2001).
- ³⁵P. Masłowski, K. F. Lee, A. C. Johansson, A. Khodabakhsh, G. Kowzan, L. Rutkowski, A. A. Mills, C. Mohr, J. Jiang, M. E. Fermann, and A. Foltynowicz, "Surpassing the path-limited resolution of Fourier-transform spectrometry with frequency combs," *Phys. Rev. A* **93**, 021802 (2016).

³⁶V. Nemtchinov, K. Sung, and P. Varanasi, "Measurements of line intensities and half-widths in the 10- μm bands of $^{14}\text{NH}_3$," J. Quant. Spectrosc. Radiat. Transf. **83**, 243–265 (2004).

³⁷E. C. Gross, K. A. Tsang, and T. J. Sears, "Re-evaluation of ortho-para-dependence of self pressure-broadening in the $\nu_1 + \nu_3$ band of acetylene," J. Chem. Phys. **154**, 054305 (2021).